MNRAS **000**, 1–11 (2016) Preprint 2 February 2016 Compiled using MNRAS LATEX style file v3.0

INTEGRAL/IBIS deep extragalactic survey: M81, LMC and 3C 273/Coma fields

Ilya A. Mereminskiy[1⋆], Roman A. Krivonos[1], Alexander A. Lutovinov[1], Sergey Yu. Sazonov[1,2], Mikhail G. Revnivtsev[1] and Rashid A. Sunyaev[1,3]
[1] *Space Research Institute, Russian Academy of Sciences, Profsoyuznaya 84/32, 117997 Moscow, Russia*
[2] *Moscow Institute of Physics and Technology, Institutsky per. 9, 141700 Dolgoprudny, Russia*
[3] *Max Planck Institute for Astrophysics, Karl-Schwarzschild-Strasse 1, D-85741 Garching, Germany*

arXiv:1602.00463v1 [astro-ph.HE] 1 Feb 2016

2 February 2016

ABSTRACT

We present results of deep surveys of three extragalactic fields, M81 (exposure of 9.7 Ms), LMC (6.8 Ms) and 3C 273/Coma (9.3 Ms), in the hard X-ray (17–60 keV) energy band with the IBIS telescope onboard the *INTEGRAL* observatory, based on 12 years of observations (2003–2015). The combined survey reaches a 4σ peak sensitivity of 0.18 mCrab (2.6×10^{-12} erg s^{-1} cm^{-2}) and sensitivity better than 0.25 and 0.87 mCrab over 10% and 90% of its full area of 4900 deg^2, respectively. We have detected in total 147 sources at $S/N > 4\sigma$, including 37 sources observed in hard X-rays for the first time. The survey is dominated by extragalactic sources, mostly by active galactic nuclei (AGN). The sample of identified sources contains 98 AGN (including 64 Seyfert galaxies, 7 LINERs, 3 XBONGs, 16 blazars and 8 AGN of unclear optical class), two galaxy clusters (Coma and Abell 3266), 17 objects located in the Large and Small Magellanic Clouds (13 high- and 2 low-mass X-ray binaries and 2 X-ray pulsars), three Galactic cataclysmic variables, one ultraluminous X-ray source (ULX, M82 X-1) and one blended source (SWIFT J1105.7+5854). The nature of 25 sources remains unknown, so that the surveys identification is currently complete at 83%. We have constructed AGN number-flux relations ($\log N$-$\log S$) and calculated AGN number densities in the local Universe for the entire survey and for each of the three extragalactic fields.

Key words: catalogues – surveys – X-rays: general.

1 INTRODUCTION

Deep X-ray surveys of extragalactic fields with focusing X-ray telescopes (see, e.g., Brandt & Alexander 2015, for a review) are essential for studying the evolution of active galactic nuclei (AGN) and physical processes powering their activity, but have a number of limitations. In particular, their small covered areas prevent finding a sufficient number of bright objects, whereas the soft X-ray energy band ($E \lesssim 10$ keV) used in most surveys introduces a strong bias against obscured (i.e. those with substantial intrinsic absorption) AGN. These drawbacks can be partially overcome using wide-field hard X-ray surveys performed with coded-mask telecopes like IBIS/*INTEGRAL* (Winkler et al. 2003) or BAT/*Swift* (Gehrels et al. 2004).

As was shown in previous studies (see e.g. Paltani et al. 2008; Krivonos et al. 2010a), the IBIS telescope aboard the *INTEGRAL* observatory is able to achieve high sensitivity in extragalactic fields. The sensitivity grows nearly proportionally to the square root of exposure showing no significant contribution of systematic noise and allowing IBIS to find sources at the tenths-of-mCrab[1] flux level with a low number of false detections. In combination with IBIS large field of view (FOV, 28°× 28°, 9°× 9° fully coded), this opens up a possibility to collect a significantly large sample of hard X-ray emitting AGN with fluxes down to a few 10^{-12} erg s^{-1} cm^{-2}. Note that such objects, due to their rarity (∼0.05 AGN per deg^2), evade *NuSTAR* deep surveys (Mullaney et al. 2015).

The observational program of *INTEGRAL* has been mainly dedicated to Galactic source studies (see, e.g., Barlow et al. 2006; Revnivtsev et al. 2008; Bodaghee et al. 2012;

⋆ E-mail:i.a.mereminskiy@gmail.com

[1] One mCrab corresponds to 1.43×10^{-11} erg s^{-1} cm^{-2} in the 17–60 keV energy band assuming a spectral shape $10(E/1keV)^{-2.1}$ photons cm^{-2} s^{-1} keV^{-1}.

© 2016 The Authors

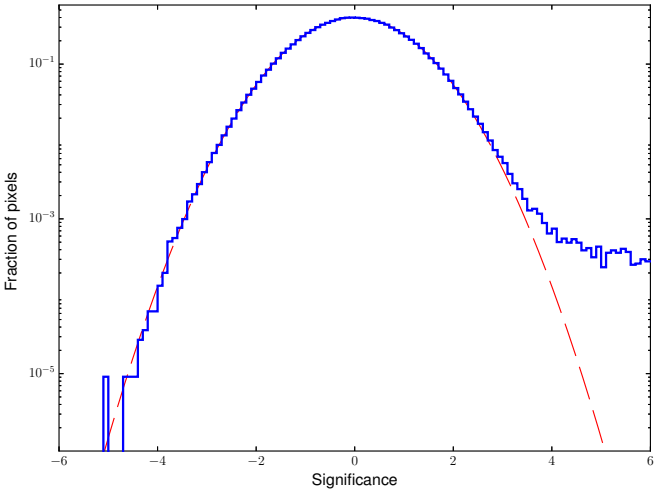

Figure 1. Distribution of pixel significances for the combined survey of three extragalactic fields (blue histogram). The red dashed line shows the normal distribution with unit variance and zero mean.

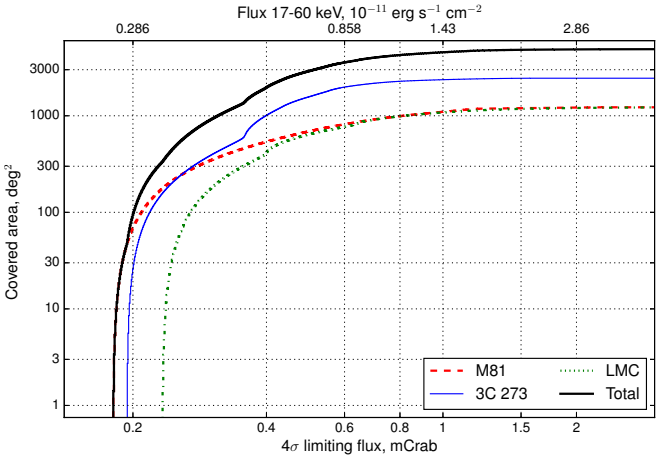

Figure 2. Sky area covered as a function of 4σ limiting flux for each field and for the combined survey.

Lutovinov et al. 2013; Walter et al. 2015), whereas the high Galactic latitude sky has been observed less intensively and very inhomogeneously. Nevertheless, on-going extragalactic surveys carried out with IBIS expand our knowledge about populations of extragalactic hard X-ray sources, mainly AGN, (Krivonos et al. 2007, 2010b; Bird et al. 2010, 2016) and provide observational input for AGN studies (Sazonov et al. 2007, 2008, 2015; Beckmann et al. 2009; Malizia et al. 2009).

A number of multi-year campaigns have been recently performed in the extragalactic sky, in particular of regions around the M81 galaxy, the Coma cluster and the Large Magellanic Cloud. In each of these fields the total accumulated exposure (per position) exceeds 3 Ms, making them interesting for population studies of extragalatic hard X-ray sources and especially AGN in the so far poorly explored domain of sub-mCrab fluxes, which is the main purpose of the present paper.

The region around the M81 and M82 galaxies was targeted during two main campaigns: the study of hard X-ray spectra of the ultraluminous X-ray sources (ULXs) HoIX X-1 and M82 X-1 (Sazonov et al. 2014) and recent observations of the type Ia supernova SN 2014J in M82 (Churazov et al. 2014). This field has a total exposure of 9.7 Ms (hereafter all quoted exposures are dead time corrected ones) at the position of the M81 galaxy.

Another *INTEGRAL* deep field, around the LMC galaxy, has a peak exposure of 6.8 Ms. The major part of the observing time was gained by the SN 1987A multi-year observational campaign (Grebenev et al. 2012). The previous hard X-ray survey of the LMC region was presented by (Grebenev et al. 2013) and had reached a peak exposure of 4.8 Ms. Note that this field is rich in X-ray binaries located in LMC/SMC.

The field around the North Galactic pole was often observed as it includes a number of interesting extragalactic sources, such as the bright AGN 3C 273 and NGC 4151 and the Coma cluster. The region of the Coma cluster was first surveyed at hard X-rays with *INTEGRAL* by Krivonos et al. (2005) who studied serendipitous extragalactic source counts down to a limiting flux of 1 mCrab. Later estimations (Krivonos et al. 2007) showed that the Coma region has an enhanced population of AGN, which probably reflects the local overdensity of AGN in the nearby Universe. This result was later confirmed by *Swift*/BAT (Ajello et al. 2012). The sky region around 3C 273/Coma (total area 2500 deg^2, exposure 4 Ms) was also selected to conduct an *INTEGRAL* extragalactic survey and to measure the source counts and AGN luminosity function (Paltani et al. 2008).

Given the IBIS FOV size and 5×5 standard observational pattern, we chose for our present study $35^\circ \times 35^\circ$ regions for the M81 and LMC fields with centers at J2000 coordinates RA=$85^\circ.0$, Dec=$-69^\circ.0$ and RA=$148^\circ.9$, Dec=$69^\circ.1$, respectively. For the 3C 273/Coma field, we chose an extended $35^\circ \times 70^\circ$ region with the aimpoint at RA=$190^\circ.0$, Dec=$17^\circ.0$ (J2000).

2 SURVEY

For the current survey we used all publicly available data acquired with *INTEGRAL* before June 2015 (spacecraft revolution 1553). The data from ISGRI, the first detector layer of the IBIS telescope, were utilized, as having the highest sensitivity at hard X-rays. We selected 17–60 keV as our working energy band where ISGRI has the highest effective area.

To apply the latest ISGRI energy calibration (Caballero et al. 2013), we first reduced the list of registered events with the *INTEGRAL* Offline Scientific Analysis (OSA) 10.1 provided by ISDC[2] up to the COR level. Then we processed the events with a proprietary analysis package developed at IKI[3] (details available in Krivonos et al. 2010a, Krivonos et al. 2012 and Churazov et al. 2014) to produce individual 17–60 keV sky images for each *INTEGRAL* science window

[2] ISDC Data Centre for Astrophysics, http://www.isdc.unige.ch/
[3] Space Research Institute of the Russian Academy of Sciences

(*ScW*), an observation with a typical duration of 2–3 ks. Finally, the list of *ScW* images was cleaned to remove noisy ones and then combined into sky mosaics.

2.1 Sensitivity and source detection

The sensitivity of the current survey is limited by photon statistics and not significantly affected by systematic noise. The distribution of S/N values for pixels from all three sky mosaic maps is shown in Fig. 1. It can be well described by pure statistical noise (at negative fluxes), which allows us to use Poisson statistics to predict the number of noise excesses above a given threshold. The combined survey covers a geometrical area of 4900 deg^2 which contains $\sim 1.2\times10^5$ independent pixels of the size of the IBIS angular resolution ($12'$). By setting a 4σ detection threshold for the current survey, we expect no more than 4 false detections in all three fields.

Fig. 2 shows the area covered by the combined survey and individual fields as a function of the 4σ limiting flux. The peak sensitivity of the survey is 0.18 mCrab (2.6×10^{-12} erg s^{-1} cm^{-2}), with 10% and 90% of the total area having been covered with sensitivity better than 0.25 mCrab (3.6×10^{-12} erg s^{-1} cm^{-2}) and 0.87 mCrab (1.2×10^{-11} erg s^{-1} cm^{-2}), respectively.

We analyzed the mosaic maps for positive excesses with $S/N > 4\sigma$ and found 147 source candidates. We cross-checked the list of the detected sources with the current *INTEGRAL* source catalog[4], the *Swift*/BAT 70-month catalog (Baumgartner et al. 2013) and the all-sky hard X-ray survey by Bird et al. (2016) as the most complete and up-to-date hard X-ray source catalogs. We also used the 66-month Palermo *Swift*/BAT online catalog[5] (Cusumano et al. 2010) as a complementary catalog. For all identified extragalactic sources we collected known redshifts or distances from the NASA/IPAC Extragalactic Database[6] (NED).

Fig. 3 shows the mosaic images along with exposure contours for the three studied fields. Note that the M81 and 3C 273/Coma fields do not show any systematic noise, which suggests that IBIS/ISGRI can be used to perform even deeper extragalactic surveys. The source statistics for each field is discussed below.

The high Galactic latitude ($b^{II} \approx 40^\circ$) M81 field contains 37 detected sources: 28 known AGN including 5 blazars, one ULX (M82 X-1), two Galactic binary systems (MU Cam and DO Dra), five new hard X-ray sources of unknown type, and SWIFT J1105.7+5854 – a known pair of sources with 6' separation (Baumgartner et al. 2013), which cannot be resolved with the IBIS telescope. This field hosts the most distant object in our survey – the quasar QSO B0836+710 at $z = 2.172$ (Stickel & Kuehr 1993). Thus, the M81 field is dominated by AGN.

In the LMC field, 46 sources are detected, including 11 objects previously unknown as hard X-ray sources. This field is different from the other two because it hosts 17 objects located in the Magellanic Clouds (both LMC and SMC), including 13 high-mass X-ray binaries, two low-mass X-ray binaries and two rotation-powered pulsars; it also contains the Galactic cataclysmic variable TW Pic. Among 21 extragalactic sources in this field there are 20 AGN, including three blazars, and the cluster of galaxies Abell 3266. The nature of 7 sources remains unknown.

In the vicinity of the bright ($\sim$20 mCrab) X-ray pulsar LMC X-4, the presence of two hard X-ray sources was reported earlier: IGR J05319−6601 (Götz et al. 2006) and IGR J05305−6559 (Krivonos et al. 2007). Due to the small angular distance from LMC X-4, these sources cannot be resolved on the average map. Nevertheless, taking into account a peculiar property of LMC X-4 (the source periodically goes to the "off"-state) and using the corresponding subset of revolutions, Grebenev et al. (2013) showed that the persistent hard X-ray emission actually originates from the sky region coinciding with the position of another X-ray pulsar, EXO 053109-6609.2. This conclusion was supported by an independent detection of this source in the standard X-ray energy band by the *INTEGRAL*/JEM-X telescope, which allowed Grebenev et al. (2013) to reconstruct the source spectrum in a broad energy band and demonstrate that it is typical for accreting X-ray pulsars. Based on the extended data set obtained with *INTEGRAL* and using the current ephemerides for LMC X-4 (Molkov et al. 2015), we have repeated such an analysis and verified the result of Grebenev et al. (2013). Summarizing the above, we can conclude that the hard X-ray emission detected by *INTEGRAL* from the vicinity of LMC X-4 is associated with the X-ray pulsar EXO 053109−6609.2 and that the hard X-ray sources IGR J05319−6601 and IGR J05305−6559 are actually the same source – the X-ray counterpart of EXO 053109−6609.2. We finally note that since our maps are averaged over many revolutions, the position and flux for this source in the catalog (referred to as IGR J05305−6559) are strongly affected by LMC X-4 and should thus be treated carefully.

The 3C 273/Coma field is the largest one and naturally contains the largest number of sources. We have detected here 64 sources including 16 objects detected in hard X-rays for the first time. All the identified sources are of extragalactic origin: there are 47 known AGN, including 7 blazars, and the Coma cluster. This field hosts the faintest object in our survey – IGR J12304+0946 with the flux of 0.21 ± 0.05 mCrab (3.0×10^{-12} erg s^{-1} cm^{-2}).

INTEGRAL has detected for the first time the galaxy cluster Abell 3266, with the flux of 0.64 ± 0.10 mCrab, confirming the previous detection by *Swift*/BAT (Ajello et al. 2009). However, unlike the Coma cluster (Lutovinov et al. 2008), the extended structure of Abell 3266 is not resolved by *INTEGRAL*. In Fig. 4, we present zoomed IBIS images of these two clusters with oveplotted contours demonstrating the 0.1–2.4 keV surface brightness, obtained from *ROSAT* data (Voges et al. 1999). Regions with the highest hard X-ray brightness coincide with the central parts of the soft X-ray images.

In summary, we have detected 147 sources in all three fields, which are listed in Table 1, including 37 detected in hard X-rays for the first time. Two fields (M81 and 3C 273/Coma) are dominated by extragalactic objects, while a significant fraction of sources in the LMC field are nearby ones (X-ray binary systems) located in LMC and SMC.

Fig. 5 shows the fluxes of the detected sources as a func-

[4] http://isdc.unige.ch/integral/catalog/39/catalog.html
[5] http://bat.ifc.inaf.it/bat_catalog_web/66m_bat_catalog.html
[6] https://ned.ipac.caltech.edu/

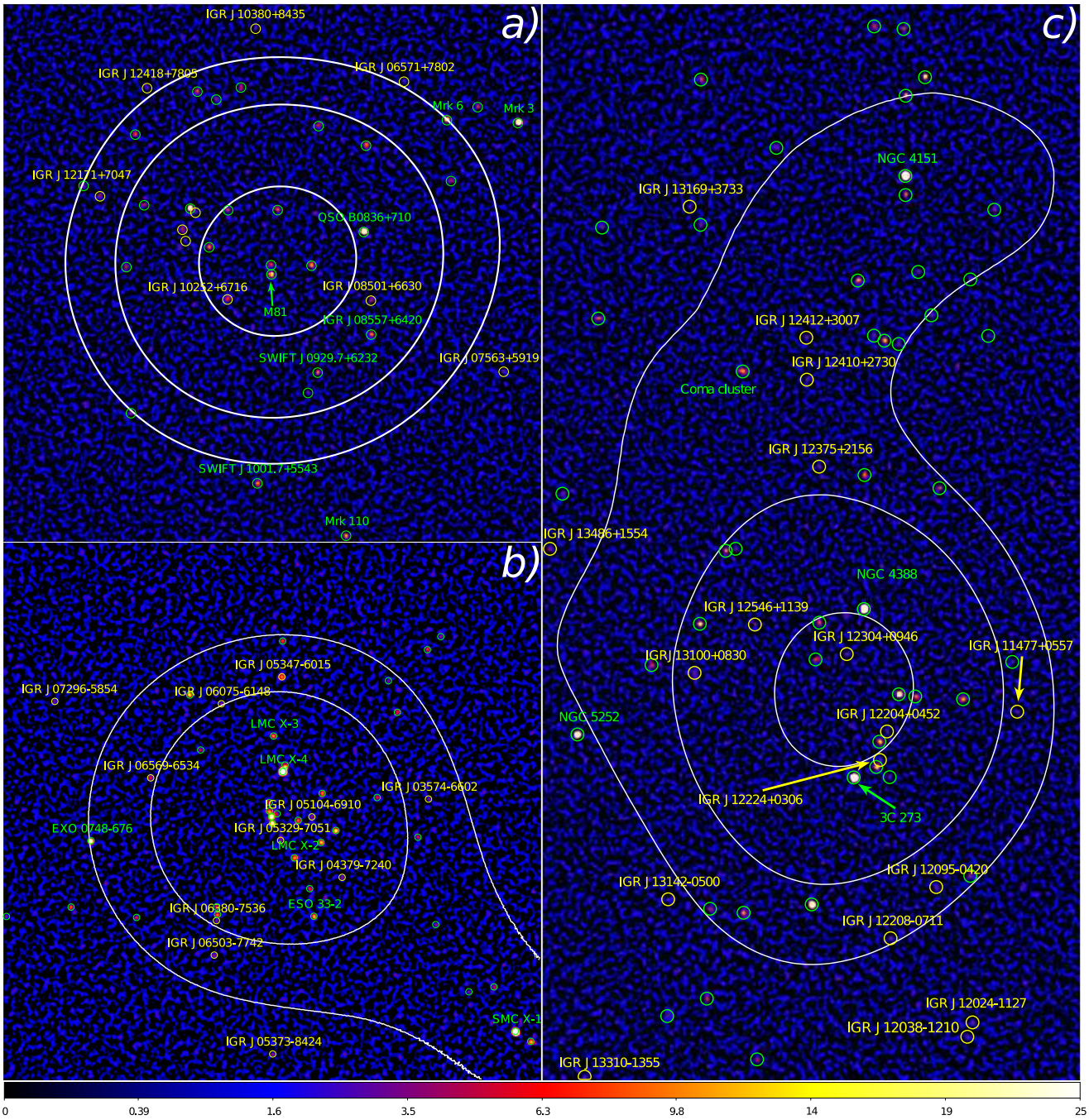

Figure 3. Hard X-ray maps of the M81, LMC and 3C 273/Coma fields, shown in terms of significance. The square-root color map ranges from 0 to 25. Yellow circles denote new sources and green circles already known ones. Some of the brightest sources are marked for easy navigation. North is up and east is to the left on all maps. *a) M81 field.* The peak exposure 9.7 Ms, contours show exposures of 2, 4 and 8 Ms. *b) LMC field.* The peak exposure 6.8 Ms, contours drawn at 2 and 4 Ms. *c) 3C 273/Coma field.* The peak exposure 9.3 Ms, contours drawn at 2, 4 and 8 Ms.

tion of the exposure time, along with an expected sensitivity curve $F_{\rm lim}^{5\sigma} = 0.77\times(T/{\rm Ms})^{-0.5}$ mCrab provided by Krivonos et al. (2010b). We see that the IBIS/ISGRI extragalactic survey continues to operate in a statistically limited regime, with the sensitivity increasing as the square root of the exposure. The factor of ~ 2 improvement in sensitivity with respect to the 7-year all-sky survey (Krivonos et al. 2010b) is clearly visible.

It is interesting to compare our catalog with an *INTEGRAL* all-sky survey catalog recently published by Bird et al. (2016) based on IBIS data taken before spacecraft orbit 1000 (December 2012). The catalog of Bird et al. (2016) contains only 65 sources out of the 147 sources detected in our survey (14/37 in the M81 field, 17/46 in LMC and 34/64 in 3C 273/Coma), which is not unexpected given that several extensive *INTEGRAL* observational campaigns of these fields have been undertaken after December 2012 and we have taken advantage of these additional data. On the

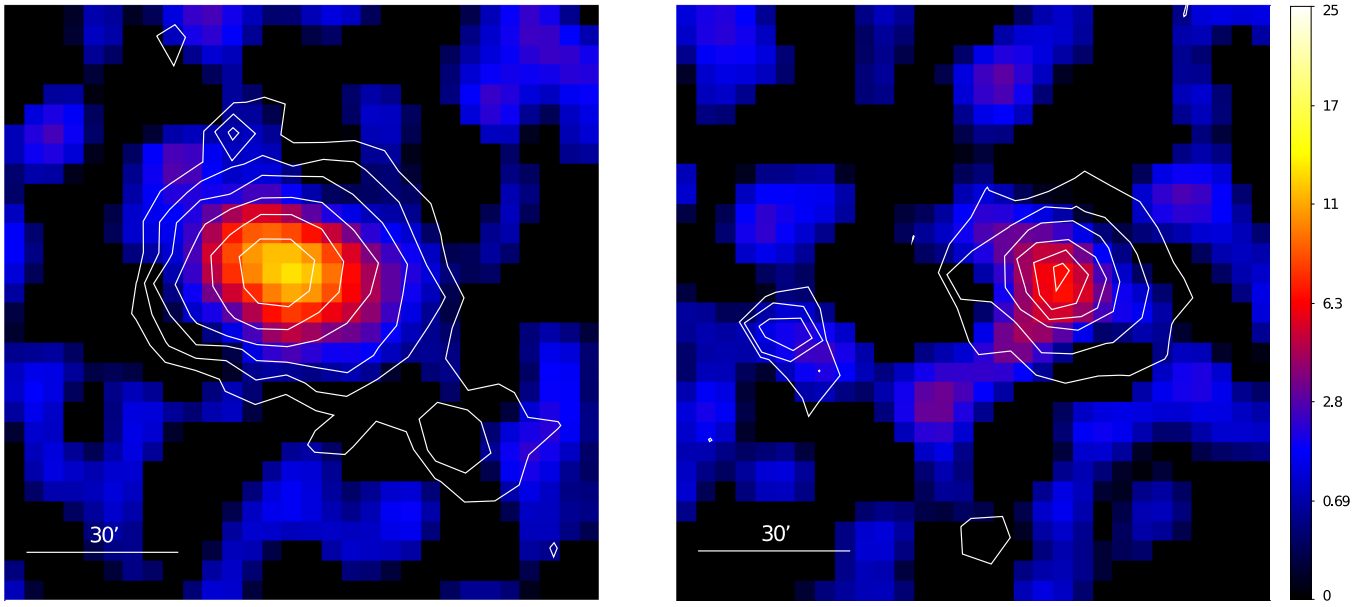

Figure 4. The 2°× 2° fields around the Coma (left) and Abell 3266 (right) clusters of galaxies. The contours denoting the surface brightness in the 0.1–2.4 keV energy band from *ROSAT* data are overplotted.

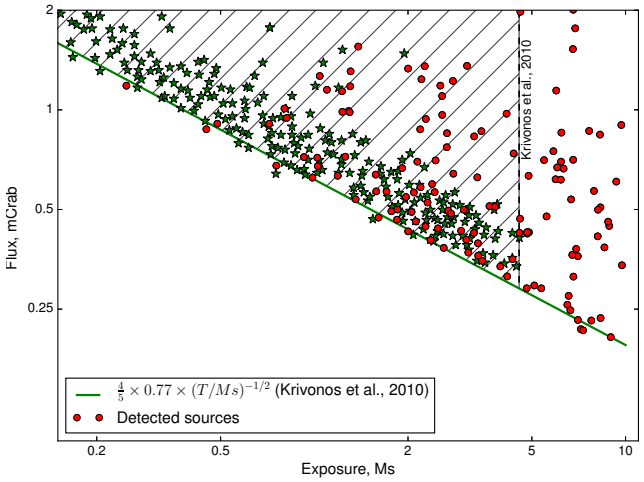

Figure 5. The 4σ limiting flux as a function of the exposure. Red circles denote sources from the current survey. Green stars are high Galactic latitude ($|b| > 15°$) sources detected in the 7-year all-sky survey (Krivonos et al. 2010b). The green line represents an analytical approximation of the nominal sensitivity versus time.

other hand, since our survey was not designed for source detection at different time scales, it misses 12 short and 3 long transients listed in Bird et al. (2016) with typical outburst timescales of weeks and months, respectively. In addition, 10 persistent weak sources from Bird et al. (2016) catalog fall below our detection threshold, including three sources in the M81 field (IGR J08447+6610, Mrk 18 and IGR J09034+5329), two in LMC (PKS 0312-770 and SWIFT J0450.7-5813) and five in 3C 273/Coma (IGR J12562+2554, IGR J13166+2340, SWIFT J1344.7+1934, IGR J12319-0749 and IGR J11486-0505), which may indicate that these sources became dimmer in the latest *INTEGRAL* observations.

2.2 Identification of new sources

For the identification of 37 newly detected sources we utilized the SIMBAD[7] and HEASARC[8] databases as well as the *Swift*/XRT point source catalog (1SXPS, Evans et al. 2014) and the third *XMM-Newton* serendipitous source catalog (3XMM-DR5, Rosen et al. 2015). Based on *XMM-Newton* or *Swift*/XRT archival observations, we selected X-ray counterparts in the soft X-ray band (2–10 keV) within a 4.2′ (2σ) error circle around the best-estimate positions of hard X-ray sources. The favored source was that which had the highest flux and a hard spectrum consistent with the *INTEGRAL* 17–60 keV flux. We found firm soft X-ray counterparts for 13 sources of 37, and list them in Table 1. In some cases we propose an optical counterpart based on positional coincidence with a known bright source, e.g. an AGN. Below we discuss a few cases of source identifications in which additional observations are needed to validate the proposed association.

IGR J08501+6630

Our search for a soft X-ray counterpart in the HEASARC archival data did not yield a potential candidate within the *INTEGRAL* error circle of IGR J08501+6630. However, we found two bright sources in optical/IR bands: the star TYC 4134-706-1 (ESA 1997) and the edge-on spiral galaxy MCG+11-11-029 ($z = 0.037$). The latter is proposed as

[7] http://simbad.u-strasbg.fr/simbad/
[8] http://heasarc.gsfc.nasa.gov/

Table 1. Part of the catalog of sources detected in the combined survey of three fields: M81, LMC and 3C 273/Coma. The descripton of the columns can be found in Sect. 2.3. The full version of the table is available in **Appendix 1**.

Id	Name[1]	R.A. deg	Dec. deg	S/N	Flux mCrab	D Mpc	z	$\log L$ erg s^{-1}	Type	Notes
				M81 field						
1	Mrk 3	93.950	71.039	39.4	5.81±0.15		0.013	43.56	Sy2	
2	IGR J06253+7334	96.370	73.585	7.6	0.99±0.13				CV	MU Cam
3	Mrk 6	103.043	74.427	22.4	2.37±0.11		0.019	43.46	Sy2	
4	**IGR J06571+7802**	104.277	78.044	4.2	0.47±0.11					
5	QSO B0716+714	110.576	71.304	5.9	0.50±0.08		0.300	45.34	Blazar	
6	**IGR J07563+5919**	119.091	59.321	4.0	0.62±0.16					
7	PG 0804+761	122.929	76.034	9.4	0.63±0.07		0.100	44.39	Sy1	
< ··· >										
147	**IGR J13486+1554**	207.168	15.901	4.8	0.57±0.12					

[1] The names of sources previously unknown in the hard X-ray band (17–60 keV) are highlighted in bold. Sources with spatial confusion are indicated by a star, their measured fluxes should be considered with caution.

Table 2. 1SXPS sources in the 4.2′ error circle around the IGR J13100+0830 position. The table is based on the 1SXPS catalog (Evans et al. 2014).

1SXPS Id	Offset[1]	R.A., Dec. (error[2])	Count rate $\times10^{-4}$ cts s^{-1} 0.2–2 keV	2–10 keV	Flux[3] $\times10^{-14}$ erg s^{-1} cm^{-2} 0.2–10 keV	Optical counterpart (type)
J131004.4+082936	1.1′	197.5184, 8.4935 (4.8″)	13.0	5.5	$7.5^{+1.8}_{-1.6}$	SDSS J131004.26+082938.9 (QSO candidate, $z = 1.22$)
J131008.5+082826	2.6′	197.5356, 8.4741 (4.4″)	13.8	3.4	$7.0^{+1.7}_{-1.5}$	SDSS J131008.34+082826.4 (galaxy, $z = 0.27$)
J131014.2+083137	3.3′	197.5592, 8.5270 (4.9″)	16.2	3.5	$8.0^{+1.8}_{-1.6}$	SDSS J131014.24+083135.9 (QSO candidate, $z = 1.55$)
J130947.2+083049	3.6′	197.4467, 8.5138 (5.3″)	5.5	1.7	$3.0^{+1.1}_{-1.0}$	USNO-B1.0 0985-0230131 (foreground star)

[1] Angular offset from the *INTEGRAL* position of IGR J13100+0830 in arcminutes.
[2] Radius of the 90% confidence error circle.
[3] The 0.2–10 keV flux (±1σ error) calculated from a power-law model with Γ=1.7 and Galactic absorption toward the source (see details in Evans et al. 2014).

a possible optical counterpart of IGR J08501+6630. The absence of a soft X-ray counterpart and non-detection of IGR J08501+6630 in the *ROSAT* all-sky survey (Voges et al. 1999) indicates a strong intrinsic absorption.

IGR J05329−7051

The error circle of IGR J05329−7051 contains one obvious soft X-ray counterpart – 3XMM J053257.8−705112, located 20″ away from the *INTEGRAL* position (Fig. 6) and having a flux of $\simeq 2 \times 10^{-13}$ erg s^{-1} cm^{-2} in the 0.2–12 keV band (Rosen et al. 2015). The optical counterpart of 3XMM J053257.8−705112 is a distant ($z = 1.238$, Kozłowski et al. 2012) AGN, MQS J053258.11−705112.9. We extracted the source spectrum from the data of an *XMM-Newton* observation in October 2001 (ObsId 0089210901, exposure 22 ks). Fitting it with the PHABS*ZPOWERLW model from the XSPEC package we obtained a low absorption column density $N_H = (1.7\pm0.8)\times10^{21}$ cm^{-2} consistent with the absorption in the Milky Way in this direction, and a moderate photon index of 2.2 ± 0.4. The corresponding model flux in the 0.2–10 keV energy range is 1.4×10^{-13} erg s^{-1} cm^{-2}. Due to its high hard X-ray luminosity $L_{17-60\ \mathrm{keV}} \sim 3\times10^{46}$ erg s^{-1} we classify this source as a candidate blazar.

IGR J13100+0830

We found four soft X-ray counterparts in the 1SXPS catalog (Evans et al. 2014) within the 4.2′ error cicrle of IGR J13100+0830, as shown in Fig. 7. Table 2 lists offsets, count rates and optical counterparts for these objects.

Because of the highest 2–10 keV flux and nearest position to the *INTEGRAL* coordinates, we propose 1SXPS J131004.4+082936 as a probable counterpart, although contribution from other sources cannot be excluded. Observations with the *NuSTAR* hard X-ray focusing tele-

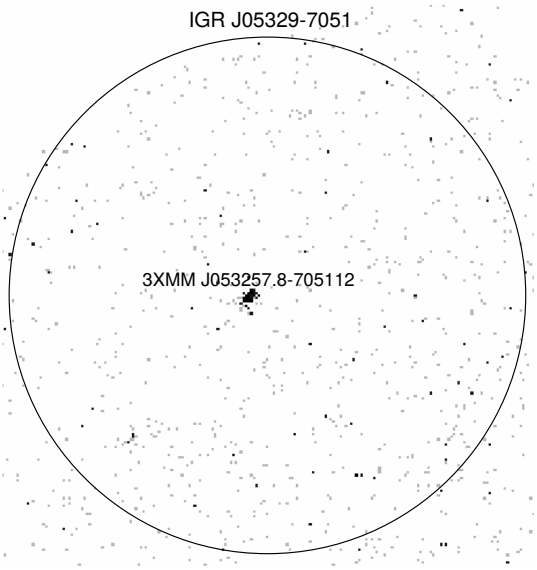

Figure 6. *XMM- Newton* EPIC MOS 0.2–10 keV image of the field around IGR J05329−7051. The circle denotes the *INTEGRAL* error region of 4.2′ in radius.

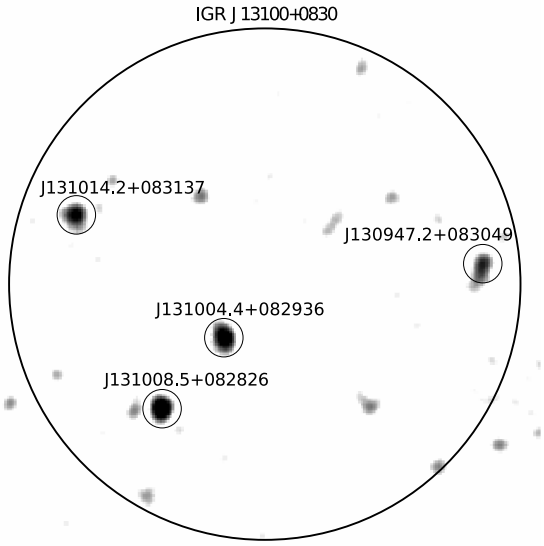

Figure 7. *Swift*/XRT 0.3–10 keV image of the field around IGR J13100+0830. The large circle of 4.2′ in radius denotes the *INTEGRAL* error region. The smaller circles denote sources from the 1SXPS catalog (Evans et al. 2014).

scope (Harrison et al. 2013) or the planned *Astro-H* mission (Takahashi et al. 2010) could help establish the nature of IGR J13100+0830 and find its optical counterpart.

2.3 Catalog

The list of the detected sources with $S/N > 4$ is presented in Table 1, which consists of three blocks corresponding to the M81, LMC and 3C 273/Coma fields. The columns of the table are described below.

Column (1) "Id" – source number in the catalog.

Column (2) "Name" – source name. For sources previously detected in hard X-rays we use their catalog or common name. We assign an "IGR" name for sources detected for the first time (also highlighed in bold).

Columns (3,4) "R.A., Dec." – right ascension and declination in equatorial coordinates (J2000 epoch).

Column (5) "S/N" – signal-to-noise ratio of the detected source.

Column (6) "Flux" – average source flux (17–60 keV) in mCrab and the associated 1σ error.

Columns (7,8) D, z – metric distance or redshift for extragalactic sources. For the calculation of luminosities (column 9) we used the metric distance for nearby sources ($z \leqslant 0.01$) and the luminosity distance estimated from the redshift for the more distant sources. Distances and redshifts were obtained from the SIMBAD and NED databases.

Column (9) $\log L$ – the logarithm of the 17–60 keV luminosity of the source. We only calculated luminosities for sources classified as AGN; a standard ΛCDM cosmology with $H_0 = 67.8$ km s^{-1} Mpc^{-1}, $\Omega_m = 0.308$ was used.

Column (10) "Type" – astrophysical type of the object: HMXB (LMXB) – high(low)-mass X-ray binary; CV – cataclysmic variable; pulsar – rotation powered X-ray pulsar; cluster – cluster of galaxies; Sy1, Sy2 (and intermediate types Sy1.2, Sy1.5, Sy1.8, Sy1.9) – Seyfert galaxies of different types; NLS1 – narrow-line Seyfert 1 galaxies; LINER – low ionization nuclear emission-line region galaxy; XBONG – X-ray bright optically normal galaxy; blazar – BL Lac object or flat-spectrum radio quasar; NLRG - narrow emission-line radio-galaxy. For all sources associated with galaxies but without known activity type we ascribe an "AGN" type.

We should note, that there are few sources which classificated as LINER based on optical observations but shows unusually high hard X-ray luminosities - more than 10^{43} erg s^{-1}, we decided to denote them as "LINER?'.'

Column (11) "Notes" – For known sources, we present an optical or IR counterpart name. For sources detected for the first time, we specify the soft X-ray counterpart and associated optical association. Some additional remarks are also provided.

3 AGN SAMPLE AND STATISTICS

Our resulting source catalog is dominated by extragalactic objects: the total sample of 98 AGN includes 64 Seyfert galaxies, 7 LINERs, 3 XBONGs, 16 blazars (or candidate blazars) and 8 AGN of unclear type. The catalog also contains 25 unidentified sources, thus the survey's identification is complete at 83%.

The *INTEGRAL*/IBIS deep extragalactic survey can be used to construct a number-flux relation for AGN, assuming that they are uniformly distributed in space (we check this assumption below). To this end, we excluded from the full AGN sample M81, NGC 4151 and 3C 273, since these were dedicated targets of long *INTEGRAL* observations, and 15 (3C 273 already excluded) blazars. The resulting sample of 80 confirmed non-blazar AGN is referred to as a *confirmed AGN sample* hereafter.

Fig. 8 shows the cumulative $\log N$–$\log S$ distribution derived from the confirmed AGN sample and corrected for the survey's sky coverage (Fig. 2). This distribution can be well described by a power law $N(>S) = AS^{-\alpha}$. Using the maximum likelihood estimator (Crawford et al. 1970) and

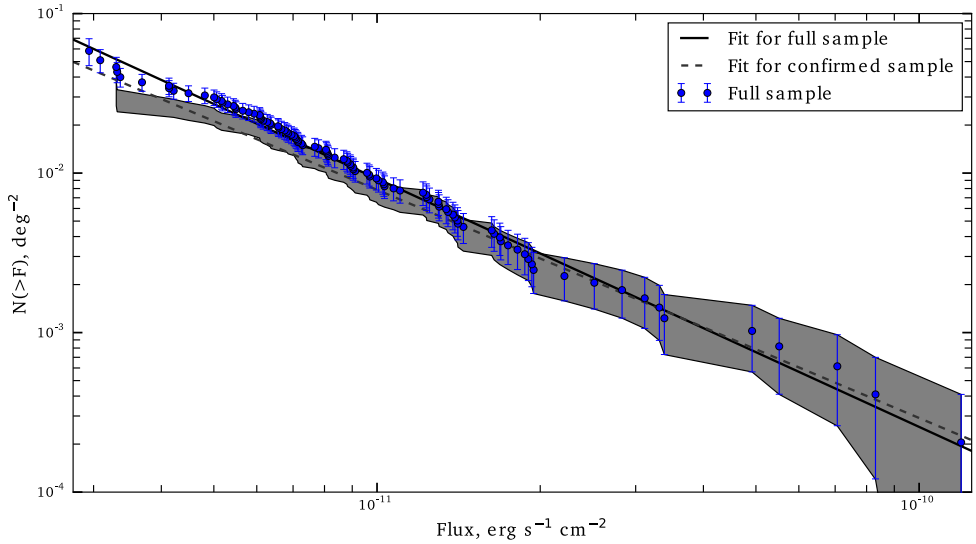

Figure 8. Number–flux (17–60 keV) relation for AGN. Blue points represent the full AGN sample (80 confirmed non-blazar AGN and 25 unidentified sources), while the black solid line shows the corresponding best-fitting power law model (the best-fit parameters are given in Table 3). The shaded area represents the 1σ error region for the confirmed AGN sample composed of 80 non-blazar AGN. The power-law fit for this sample is shown by the gray dashed line.

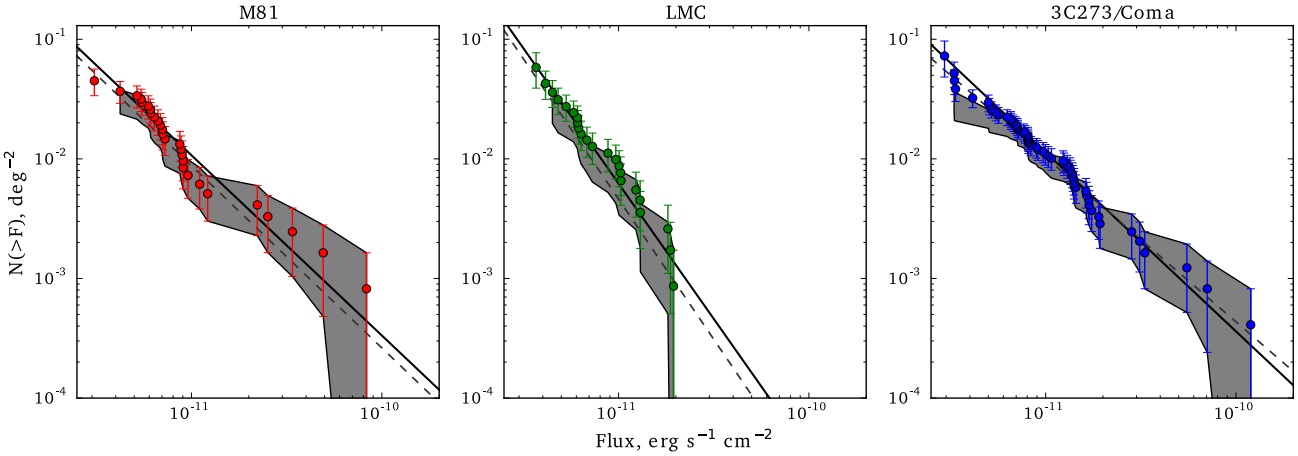

Figure 9. Number–flux (17–60 keV) relations for sources in the three extragalactic fields. The colored dots show both known non-blazar AGN and unidentified sources, and the black solid lines represent the corresponding power-law fits (the parameter values are given in Table 3). The shaded areas represent the 1σ regions of best-fit parameters excluding unidentified sources. Power-law fits for samples without unidentified sources are shown as dashed gray lines.

the source number counts, we determined the slope $\alpha = 1.44 \pm 0.14$ and normalization $A = (2.9 \pm 0.3) \times 10^{-3}$ deg^{-2}, at the flux 2×10^{-11} erg s^{-1} cm^{-2}, of the number-flux relation. Although the derived slope is consistent with that (3/2) expected for homogeneously distributed objects, there is an indication of some flattening of the $\log N$–$\log S$ distribution below $\simeq 6 \times 10^{-12}$ erg s^{-1} cm^{-2}, which may be caused by the incompleteness of our survey at these low fluxes.

Taking into account the high Galactic latitudes of the extragalactic fields under consideration, it is reasonable to expect that most of the unidentified sources in our sample have an extragalactic nature. We therefore also constructed a larger *full AGN sample* by adding all 25 unidentified sources to our confirmed AGN sample. The new sample includes 105 hard X-ray sources spanning down to a flux of $\simeq 3 \times 10^{-12}$ erg s^{-1} cm^{-2}, which is a factor of two deeper than the all-sky extragalactic $\log N$–$\log S$ relation constructed by Krivonos et al. (2010b). Using the same approach as before, we derived the best-fit slope $\alpha = 1.56 \pm 0.13$ and normalization $A = (3.1 \pm 0.3) \times 10^{-3}$ deg^{-2} at the flux of 2×10^{-11} erg s^{-1} cm^{-2} for the number-flux relation constructed from the full AGN sample (see Fig. 8 and

Table 3). These values are not significantly different from our estimates based on the confirmed AGN sample. The derived slope is consistent with 3/2, while the normalization is slightly lower but still consistent with the value of $(3.59 \pm 0.35) \times 10^{-3}$ deg^{-2} obtained for the all-sky *INTEGRAL* survey by Krivonos et al. (2010b).

We further used the full AGN sample to construct the $\log N$–$\log S$ distributions for the three individual extragalactic fields (Fig. 9). The corresponding slopes and normalizations are summarized in Table 3. The slopes and normalizations for the M81 and 3C 273/Coma fields are compatible with each other while the LMC field shows a significantly steeper slope, yet consistent within 2σ with the $\log N$–$\log S$ fit for the combined survey. The apparent lack of bright ($> 2{\times}10^{-11}$ erg s^{-1} cm^{-2}) AGN in the direction of the Large Magellanic Cloud was previously noticed by Lutovinov et al. (2012).

It is well known that the spatial distribution of galaxies in the local Universe is strongly inhomogeneous on scales less than $\sim$ 100–200 Mpc (Jarrett 2004). With the typical sensitivity of our deep *INTEGRAL*/IBIS survey $\sim 5 \times 10^{-12}$ erg s^{-1} cm^{-2} (17–60 keV) we can detect AGN with the characteristic luminosity of $L_* \sim 5 \times 10^{43}$ erg s^{-1} (Sazonov et al. 2007, 2015) beyond this scale, out to $\sim$ 300 Mpc. This fact is confirmed by Fig. 10, where we plot the hard X-ray luminosity vs. redshift for the confirmed AGN sample. Therefore, we can make use of the AGN count statistics in the directions to M81, LMC and 3C 273/Coma fields to probe the matter distribution in the local Universe regarding AGN as its tracers (Krivonos et al. 2007; Ajello et al. 2012).

To get a rough idea, we can compare the numbers of nearby AGN (at distances $D < 150$ Mpc) found in the three fields (see Table 3). There are 12 such objects (i.e. confirmed non-blazar AGN) in the M 81 field, 5 in the LMC field and 27 in the 3C 273/Coma field. Given that the last field is two times larger than the former two, these numbers do not indicate a significant difference in the AGN space density in the three considered directions. More accurate estimates can be achieved with the $1/V_{max}$ method (Schmidt 1968; Huchra & Sargent 1973). We restricted our analysis to sources with $D < 150$ Mpc and L$>10^{42}$ erg s^{-1} (within the shaded region in Fig. 10). The latter condition is imposed to diminish the statistical noise associated with the lowest luminosity (and hence very nearby) AGN. The resulting samples contain 9, 4 and 18 AGN in the M 81, LMC and 3C 273/Coma fields, respectively. As can be seen from Table 3, the LMC field exhibits the lowest local AGN space density. However, the estimated densities for the different fields are consistent with the density estimated by combining these fields.

4 SUMMARY

We have analyzed the deepest *INTEGRAL* hard X-ray survey of three extragalactic fields: around M81, LMC and 3C 273/Coma, with the peak exposure of 6.8 Ms in the LMC field and above 9 Ms in the two other fields. The peak achieved sensitivity is 0.18 mCrab in the 17–60 keV energy band. The catalog of sources detected in the combined survey contains 147 objects detected above the threshold of $S/N > 4$, with 37 of them having been detected in hard X-rays for the first time. We have identified 13 of the newly detected objects using archival soft X-ray observations. Twenty five sources (24 of new and SWIFT J0826.2–7033) remain unidentified making the completeness of the survey at the level of 83%.

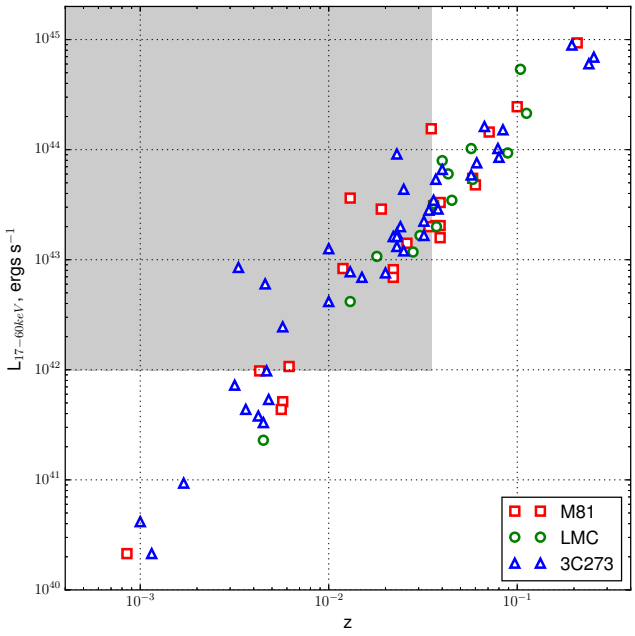

Figure 10. Hard X-ray luminosty vs. redshift for the identified non-blazar AGN. The sources from shaded region were used for estimating the AGN space density (see text for details).

The catalog is dominated by extragalactic sources. The cumulative $\log N$–$\log S$ distribution of non-blazar AGN is consistent with a power law down to fluxes $\simeq 3 \times 10^{-12}$ erg s^{-1} cm^{-2}, which is deeper by a factor of two compared to the previous (all-sky) measurement of Krivonos et al. (2010b). The AGN number counts for the M81 and 3C 273/Coma fields are consistent with each other, while the LMC field demonstrates a steeper number-flux distribution (2σ deviation from the expected $-3/2$ slope) and a lack of bright AGN with flux higher than $2{\times}10^{-11}$ erg s^{-1} cm^{-2}.

ACKNOWLEDGEMENTS

This work is based on observations with *INTEGRAL*, an ESA project with instruments and the science data centre funded by ESA member states (especially the PI countries: Denmark, France, Germany, Italy, Switzerland, Spain), and Poland, and with the participation of Russia and the USA. The data were obtained from the European[9] and Russian[10] *INTEGRAL* Science Data Centers. This research was supported by the Russian Science Foundation (grant 14-22-00271). The authors thank the Max-Planck-Institut für Astrophysik for computational support.

[9] http://isdc.unige.ch
[10] http://hea.iki.rssi.ru/rsdc

Table 3. Best–fit parameters for the number-flux relations and estimated AGN space densities.

Parameter	Units	M81	LMC	3C 273/Coma	Total
$\log N$–$\log S$, best-fit parameters for full AGN sample (confirmed AGN and unidentified sources)					
α		1.51±0.23	2.26±0.36	1.50±0.17	1.56 ± 0.13
A^1	$\times 10^{-3}$ deg^{-2}	3.8±0.7	1.3±0.3	4.0±0.5	3.1 ± 0.3
N^2		27	23	55	105
$\log N$–$\log S$, best-fit parameters for confirmed AGN sample					
α		1.52±0.27	2.34±0.46	1.37±0.19	1.43 ± 0.14
A^1	$\times 10^{-3}$ deg^{-2}	3.0±0.6	0.9±0.2	4.0±0.6	2.9 ± 0.3
N^3		22	16	42	80
N^4		12	5	27	44
N^5		9	4	18	31
AGN space density estimated by the $1/V_{max}$ method					
ρ^6	$\times 10^{-5}$ Mpc^{-3}	14.8±11.6	3.2±2.1	5.4 ± 2.1	7.6 ± 3.5

[1] The normalization A is derived at the flux 2×10^{-11} erg s^{-1} cm^{-2}.
[2] The number of confirmed non-blazar AGN and unidentified sources in the field.
[3] The number of confirmed non-blazar AGN in the field.
[4] The number of confirmed non-blazar AGN at $D < 150$ Mpc.
[5] The number of confirmed non-blazar AGN at $D < 150$ Mpc with $L > 10^{42}$ erg s^{-1}.
[6] Number density of AGN at $D < 150$ Mpc with $L > 10^{42}$ erg s^{-1}.

REFERENCES

Ajello M., et al., 2009, ApJ, 690, 367
Ajello M., Alexander D. M., Greiner J., Madejski G. M., Gehrels N., Burlon D., 2012, ApJ, 749, 21
Barlow E. J., Knigge C., Bird A. J., J Dean A., Clark D. J., Hill A. B., Molina M., Sguera V., 2006, MNRAS, 372, 224
Baumgartner W. H., Tueller J., Markwardt C. B., Skinner G. K., Barthelmy S., Mushotzky R. F., Evans P. A., Gehrels N., 2013, ApJS, 207, 19
Beckmann V., et al., 2009, A&A, 505, 417
Bird A. J., et al., 2010, ApJ, 186, 1
Bird A. J., et al., 2016, preprint, (arXiv:1601.06074)
Bodaghee A., Tomsick J. A., Rodriguez J., James J. B., 2012, ApJ, 744, 108
Brandt W. N., Alexander D. M., 2015, AApR, 23, 1
Caballero I., et al., 2013, preprint, (arXiv:1304.1349)
Churazov E., et al., 2014, Nature, 512, 406
Crawford D. F., Jauncey D. L., Murdoch H. S., 1970, ApJ, 162, 405
Cusumano G., et al., 2010, A&A, 524, A64
ESA ed. 1997, The HIPPARCOS and TYCHO catalogues. Astrometric and photometric star catalogues derived from the ESA HIPPARCOS Space Astrometry Mission ESA Special Publication Vol. 1200
Evans P. A., et al., 2014, ApJS, 210, 8
Gehrels N., et al., 2004, ApJ, 611, 1005
Götz D., Mereghetti S., Merlini D., Sidoli L., Belloni T., 2006, A&A, 448, 873
Grebenev S. A., Lutovinov A. A., Tsygankov S. S., Winkler C., 2012, Nature, 490, 373
Grebenev S. A., Lutovinov A. A., Tsygankov S. S., Mereminskiy I. A., 2013, MNRAS, 428, 50
Harrison F. A., et al., 2013, ApJ, 770, 103
Huchra J., Sargent W. L. W., 1973, ApJ, 186, 433
Jarrett T., 2004, PASA, 21, 396
Kozłowski S., et al., 2012, ApJ, 746, 27
Krivonos R., Vikhlinin A., Churazov E., Lutovinov A., Molkov S., Sunyaev R., 2005, ApJ, 625, 89
Krivonos R., Revnivtsev M., Lutovinov A., Sazonov S., Churazov E., Sunyaev R., 2007, A&A, 475, 775
Krivonos R., Revnivtsev M., Tsygankov S., Sazonov S., Vikhlinin A., Pavlinsky M., Churazov E., Sunyaev R., 2010a, A&A, 519, A107
Krivonos R., Tsygankov S., Revnivtsev M., Grebenev S., Churazov E., Sunyaev R., 2010b, A&A, 523, A61
Krivonos R., Tsygankov S., Lutovinov A., Revnivtsev M., Churazov E., Sunyaev R., 2012, A&A, 545, A27
Lutovinov A. A., Vikhlinin A., Churazov E. M., Revnivtsev M. G., Sunyaev R. A., 2008, ApJ, 687, 968
Lutovinov A. A., Grebenev S. A., Tsygankov S. S., 2012, Astronomy Letters, 38, 492
Lutovinov A. A., Revnivtsev M. G., Tsygankov S. S., Krivonos R. A., 2013, MNRAS, 431, 327
Malizia A., Stephen J. B., Bassani L., Bird A. J., Panessa F., Ubertini P., 2009, MNRAS, 399, 944
Molkov S. V., Lutovinov A. A., Falanga M., 2015, Astronomy Letters, 41, 562
Mullaney J. R., et al., 2015, ApJ, 808, 184
Paltani S., Walter R., McHardy I. M., Dwelly T., Steiner C., Courvoisier T. J.-L., 2008, A&A, 485, 707
Revnivtsev M., Lutovinov A., Churazov E., Sazonov S., Gilfanov M., Grebenev S., Sunyaev R., 2008, A&A, 491, 209
Rosen S. R., et al., 2015, preprint, (arXiv:1504.07051)
Sazonov S., Revnivtsev M., Krivonos R., Churazov E., Sunyaev R., 2007, A&A, 462, 57
Sazonov S., Krivonos R., Revnivtsev M., Churazov E., Sunyaev R., 2008, A&A, 482, 517
Sazonov S. Y., Lutovinov A. A., Krivonos R. A., 2014, Astronomy Letters, 40, 65
Sazonov S., Churazov E., Krivonos R., 2015, MNRAS, 454, 1202
Schmidt M., 1968, ApJ, 151, 393
Stickel M., Kuehr H., 1993, A&AS, 100, 395
Takahashi T., et al., 2010, in Society of Photo-Optical Instrumentation Engineers (SPIE) Conference Series. p. 0 (arXiv:1010.4972), doi:10.1117/12.857875
Voges W., et al., 1999, A&A, 349, 389

Walter R., Lutovinov A. A., Bozzo E., Tsygankov S. S., 2015, A&ARv, 23, 2
Winkler C., et al., 2003, A&A, 411, L1

Appendix 1. The complete catalog of hard X-ray sources detected in the combined survey of three fields: M81, LMC and 3C 273/Coma. The descripton of the columns can be found in Sect. 2.3 of the paper.

Id	Name[1]	R.A. deg	Dec. deg	S/N	Flux mCrab	D Mpc	z	$\log L$ erg s^{-1}	Type	Notes
					M81 field					
1	Mrk 3	93.950	71.039	39.4	5.81±0.15		0.013	43.56	Sy2	
2	IGR J06253+7334	96.370	73.585	7.6	0.99±0.13				CV	MU Cam
3	Mrk 6	103.043	74.427	22.4	2.37±0.11		0.019	43.46	Sy2	
4	**IGR J06571+7802**	104.277	78.044	4.2	0.47±0.11					
5	QSO B0716+714	110.576	71.304	5.9	0.50±0.08		0.300	45.34	Blazar	
6	**IGR J07563+5919**	119.091	59.321	4.0	0.62±0.16					
7	PG 0804+761	122.929	76.034	9.4	0.63±0.07		0.100	44.39	Sy1	
8	QSO B0836+710	130.333	70.905	62.2	3.27±0.05		2.172	48.24	Blazar	
9	**IGR J08501+6630**	132.547	66.515	6.9	0.38±0.06					
10	IGR J08557+6420	133.839	64.391	11.2	0.67±0.06		0.036	43.49	Sy2	MCG +11-11-032
11	NGC 2655	133.901	78.250	6.3	0.43±0.07	24.4		41.64	LINER	
12	Mrk 110	141.292	52.292	12.2	3.44±0.28		0.035	44.19	Sy1	
13	IGR J09253+6929	141.455	69.481	13.1	0.61±0.05		0.039	43.52	Sy1.5	2MASX J09254750+6927532
14	SWIFT J0929.7+6232	142.413	62.556	10.2	0.62±0.06		0.026	43.15	Sy2	2MASX J09293791+6232382
15	SWIFT J0935.9+6120	143.991	61.314	4.5	0.29±0.07		0.039	43.20	Sy1	MCG +10-14-025
16	SWIFT J0950.5+7318	147.509	73.248	9.3	0.45±0.05		0.058	43.74	Sy2/NLRG	VII Zw 292
17	M81	148.898	69.080	19.8	0.90±0.05	3.7		40.33	LINER	
18	M82 X–1	148.973	69.675	7.5	0.34±0.05				ULX	
19	SWIFT J1001.7+5543	150.489	55.709	11.7	1.55±0.13	19.1		41.99	Sy2	NGC 3079
20	**IGR J10252+6716**	156.324	67.273	7.9	0.38±0.05		0.039	43.31	Sy2	2RXP J102510.2+671801, KUG 1021+675
21	SWIFT J1033.6+7303	158.576	73.016	8.3	0.41±0.05		0.022	42.84	XBONG	CGCG 333-038
22	**IGR J10380+8435**	159.513	84.587	4.4	0.63±0.14					
23	SWIFT J1044.1+7024	161.072	70.431	10.2	0.51±0.05		0.034	43.3	Sy2	MCG +12-10-067
24	QSO J1044+8054	161.240	80.862	5.7	0.50±0.09		1.260	46.84	Blazar	
25	**IGR J11015+7224**	165.392	72.409	4.0	0.22±0.05		1.459	46.64	Blazar	1SXPS J110148.6+722534, 4C 72.16
26	**IGR J11030+7027**	165.758	70.463	4.1	0.22±0.05					1RXS J110257.6+702948
27	SWIFT J1105.7+5854	166.456	58.913	6.0	0.67±0.11					Double source (Sy2+blazar)
28	NGC 3516	166.694	72.566	31.9	1.76±0.06	52.5		42.92	Sy1.5	
29	**IGR J11079+7106**	166.992	71.109	6.6	0.36±0.05		0.060	43.68	AGN	1RXS J110748.8+710538, 2MASX J11074777+7105326
30	SWIFT J1114.3+7944	168.978	79.698	5.0	0.42±0.08		0.037	43.31	Sy2	MCG +13-08-056
31	SWIFT J1136.7+6738	174.155	67.595	6.8	0.47±0.07		0.134	44.53	Blazar	2MASX J11363009+6737042
32	SWIFT J1142.7+7149	175.909	71.686	6.2	0.42±0.07				CV	DO Dra
33	SWIFT J1143.7+7942	176.199	79.681	9.1	0.85±0.09	27.2		42.03	Sy1.2	UGC 06728
34	**IGR J12171+7047**	184.288	70.797	5.2	0.48±0.09	25.0		41.71	AGN	1SXPS J121726.3+704806,

Continued on next page

Table 4 – continued from previous page

Id	Name[1]	R.A. deg	Dec. deg	S/N	Flux mCrab	D Mpc	z	log L erg s^{-1}	Type	Notes
										NGC 4250
35	Mrk 205	185.440	75.305	8.2	0.77±0.09		0.071	44.16	Sy1	
36	3PBC J1231.3+7044	187.944	70.746	4.6	0.49±0.11		0.208	44.97	Sy1.2	2MASS J12313656+7044144
37	**IGR J12418+7805**	190.462	78.084	4.2	0.49±0.12		0.022	42.91	Sy1.9	RX J1242.8+7807, NPM1G +78.0048
					LMC field					
38	IGR J01054–7253	16.223	-72.886	12.4	1.24±0.10				HMXB	2MASS J01044227-7254036
39	SMC X–1	19.285	-73.441	179.0	17.72±0.10				HMXB	
40	SWIFT J0157.8–7300	29.284	-73.063	5.2	0.52±0.10				HMXB	USNO-B1.0 0170-00064697
41	SWIFT J0208.4–7428	31.675	-74.470	4.0	0.40±0.10				HMXB	
42	SWIFT J0308.5–7251	46.950	-72.819	4.6	0.43±0.09		0.028	43.07	Sy1.2	ESO 031-8
43	IGR J03532–6829	58.344	-68.556	6.1	0.51±0.08		0.087	44.17	Blazar	PKS 0352-686
44	**IGR J03574–6602**	59.375	-66.043	4.0	0.37±0.09					
45	SWIFT J0422.7–5611	65.542	-56.183	4.5	0.91±0.20		0.043	43.78	Sy2	ESO 157-23
46	1H 0419–577	66.533	-57.184	7.6	1.27±0.17		0.104	44.73	Sy1.5	2MASS J04260071-5712017
47	IGR J04288–6702	67.194	-67.075	6.0	0.43±0.07					
48	Abell 3266	67.869	-61.462	6.6	0.64±0.10		0.059	43.91	Cluster	
49	**IGR J04379–7240**	69.492	-72.669	4.3	0.29±0.07					
50	SWIFT J0440.2–5941	70.056	-59.662	4.1	0.44±0.11		0.058	43.73	Sy2	ESO 118-033
51	SWIFT J0451.5–6949	72.811	-69.795	18.2	1.14±0.06				HMXB	
52	ESO 033–G002	74.014	-75.526	12.7	0.91±0.07		0.018	43.03	Sy2	
53	IGR J05007–7047	75.235	-70.739	13.9	0.85±0.06				HMXB	
54	SWIFT J0504.6–7345	76.108	-73.810	7.3	0.48±0.07		0.045	43.54	Sy1.9	2MASX J05043414-7349269
55	SWIFT J0505.6–6735	76.365	-67.567	10.0	0.62±0.06				AGN	2MASX J05052442-6734358
56	**IGR J05104–6910**	77.622	-69.170	4.3	0.26±0.06					
57	RX J0520.5–6932	80.060	-69.480	9.1	0.54±0.06				HMXB	[HP99] 946
58	LMC X–2	80.225	-71.939	10.9	0.66±0.06				LMXB	
59	IGR J05305–6559*	82.864	-65.935	11.2	0.70±0.06				HMXB	
60	LMC X–4	83.197	-66.371	334.7	20.33±0.06				HMXB	2MASS J05324953-6622132
61	**IGR J05329–7051**	83.226	-70.853	4.2	0.25±0.06		1.238	46.52	Blazar?	3XMM J053257.8-705112, MQS J053258.11-705112.9
62	IGR J05346–5759	83.674	-57.992	7.9	0.87±0.11				CV	TW Pic
63	**IGR J05347–6015**	83.678	-60.258	10.0	0.86±0.09		0.057	44.01	Sy1	1SXPS J053430.8-601617, 2MASX J05343093-6016153
64	PSR J0537–6910	84.008	-69.124	8.2	0.31±0.06				Pulsar	
65	**IGR J05373–8424**	84.342	-84.408	4.5	0.72±0.16					
66	LMC X–3	84.714	-64.069	10.7	0.70±0.07				HMXB	
67	LMC X–1	84.856	-69.759	26.1	1.53±0.06				HMXB	2MASS J05393883-6944356
68	PSR B0540–69.3	85.017	-69.327	34.4	2.01±0.06				Pulsar	

Continued on next page

Table 4 – continued from previous page

Id	Name[1]	R.A. deg	Dec. deg	S/N	Flux mCrab	D Mpc	z	log L erg s^{-1}	Type	Notes
69	IGR J05414–6858*	85.387	-68.944	12.0	0.71±0.06				HMXB	
70	SWIFT J0541.5–6826	85.420	-68.398	6.2	0.36±0.06				HMXB	XMMU J054134.7-682550
71	**IGR J06075–6148**	91.899	-61.814	4.2	0.34±0.08	19.9		41.36	AGN	3XMM J060730.3-614827, ESO 121–G006
72	SWIFT J0623.3–6438	95.784	-64.580	6.0	0.43±0.07		0.129	44.46	Blazar	2MASX J06230765-6436211
73	IGR J06239–6052	95.925	-60.987	14.8	1.36±0.09		0.040	43.90	Sy2	ESO 121-28
74	SWIFT J0634.7–7445	98.712	-74.764	5.8	0.43±0.07		0.112	44.33	Sy1	2MASS J06340353-7446377
75	IGR J06354–7516	98.892	-75.249	9.8	0.74±0.08		0.653	46.31	Blazar	PKS 0637-752
76	**IGR J06380–7536**	99.525	-75.616	4.1	0.31±0.08		0.089	43.97	Sy1.8	2E 0639.5-7535, 2MASX J06374318-7538458
77	**IGR J06503–7742**	102.599	-77.701	4.4	0.41±0.09		0.0373	43.30	AGN	XMMSL1 J064954.6-774216, 2MASX J06495436-7742143
78	**IGR J06569–6534**	104.240	-65.570	6.2	0.51±0.08		0.0305	43.22	Sy1	RX J065630-65349, Fairall 265
79	**IGR J07296–5854**	112.413	-58.905	4.2	0.72±0.17					
80	SWIFT J0747.6–7326	116.989	-73.449	6.8	0.70±0.10		0.036	43.51	LINER?	2MASX J07473839-7325533
81	EXO 0748–676	117.097	-67.756	28.7	3.25±0.11				LMXB	
82	SWIFT J0826.2–7033	126.584	-70.527	9.2	1.31±0.14					1SXPS J082623.1-703143
83	IGR J09025–6814	135.680	-68.219	4.3	0.68±0.15		0.013	42.62	XBONG	NGC 2788A
	3C 273/Coma field									
84	SWIFT J1144.1+3652	176.118	36.924	5.9	0.56±0.10		0.038	43.46	Sy1	KUG 1141+371
85	**IGR J11477+0557**	176.931	5.966	4.6	0.40±0.09					
86	SWIFT J1148.3+0901	177.025	9.049	4.2	0.35±0.08		0.069	43.79	Sy1.5	2MASX J11475508+0902284
87	SWIFT J1148.7+2941	177.171	29.609	5.1	0.72±0.14		0.023	43.12	Sy1	MCG +05-28-032
88	3PBC J1152.9+3307	178.186	33.104	4.0	0.43±0.11		1.398	46.89	Blazar	7C 1150+3324
89	SWIFT J1200.8+0650	180.237	6.810	11.9	0.75±0.06		0.036	43.54	Sy2	2MASX J12005792+0648226
90	SWIFT J1201.2–0341	180.334	-3.696	5.6	0.58±0.10		0.020	42.88	Sy1	Mrk 1310
91	**IGR J12024–1127**	180.622	-11.460	4.3	0.91±0.21					
92	NGC 4051	180.769	44.522	19.9	2.18±0.11	14.0		41.86	Sy1	NGC 4051
93	**IGR J12038–1210**	180.958	-12.178	4.0	0.87±0.22					
94	NGC 4074	181.115	20.324	8.8	0.94±0.11		0.022	43.21	Sy2	NGC 4074
95	3PBC J1204.7+3109	181.121	31.193	4.9	0.55±0.11		0.025	43.08	Sy1.9	UGC 7064
96	SWIFT J1207.5+3355	181.949	33.854	4.6	0.44±0.10		0.079	44.01	Sy2	B2 1204+34
97	SWIFT J1209.5+4702	182.323	47.036	7.3	0.98±0.13		0.024	43.30	Sy2	Mrk 198
98	NGC 4138	182.363	43.688	12.8	1.33±0.10	20.7		41.99	Sy1.9	
99	**IGR J12095–0420**	182.394	-4.344	4.0	0.38±0.09					
100	NGC 4151	182.628	39.408	305.2	27.67±0.09	13.4		42.93	Sy1.5	NGC 4151
101	IGR J12107+3822	182.671	38.343	10.8	0.97±0.09		0.023	43.24	Sy1.5	KUG 1208+386
102	NGC 4180	183.253	7.036	10.7	0.57±0.05	39.2		41.97	LINER	

Continued on next page

Table 4 – continued from previous page

Id	Name[1]	R.A. deg	Dec. deg	S/N	Flux mCrab	D Mpc	z	log L erg s^{-1}	Type	Notes
103	Was 49	183.571	29.578	5.2	0.56±0.11		0.061	43.88	Sy1	
104	IGR J12172+0710	184.302	7.187	45.3	2.32±0.05	25.0		42.39	Sy1.2	NGC 4235
105	Mrk 766	184.600	29.828	13.2	1.35±0.10		0.013	42.89	Sy1	
106	NGC 4258	184.727	47.298	7.1	0.99±0.14	7.5		40.97	Sy2	
107	3PBC J1220.1+0203	185.022	2.065	4.1	0.23±0.06		0.240	44.78	Sy1.8	PKS 1217+023
108	**IGR J12204+0452**	185.120	4.868	4.6	0.24±0.05					
109	**IGR J12208–0711**	185.212	-7.192	4.5	0.46±0.10					
110	QSO B1218+304	185.351	30.169	6.0	0.60±0.10		0.184	44.94	Blazar	
111	**IGR J12224+0306**	185.606	3.110	4.3	0.23±0.05		0.255	44.84	QSO?	1SXPS J122208.8+030717, SDSS J122208.78+030718.4
112	4C 04.42	185.620	4.239	16.3	0.84±0.05		0.966	46.78	Blazar	
113	Mrk 50	185.851	2.689	16.0	0.86±0.05		0.023	43.21	Sy1.2	
114	QSO B1222+216	186.234	21.363	9.5	0.83±0.09		0.433	45.93	Blazar	
115	NGC 4388	186.449	12.663	155.7	8.36±0.05	20.6		42.78	Sy2	
116	NGC 4395	186.456	33.552	13.6	1.22±0.09	4.5		40.62	Sy1.8	
117	3C 273	187.279	2.052	249.7	13.46±0.05		0.158	46.15	Blazar	
118	**IGR J12304+0946**	187.620	9.776	4.2	0.21±0.05					
119	**IGR J12375+2156**	189.392	21.944	4.3	0.36±0.08					
120	NGC 4579	189.412	11.804	9.5	0.50±0.05	19.8		41.52	LINER?	
121	SWIFT J1238.6+0928	189.665	9.440	9.2	0.46±0.05		0.032	43.22	AGN	VCC 1759
122	NGC 4593	189.925	-5.356	47.3	3.86±0.08	44.0		43.10	Sy1	
123	SWIFT J1240.9+2735	190.260	27.505	5.4	0.50±0.09		0.057	43.77	Sy2	KUG 1238+278A
124	**IGR J12412+3007**	190.302	30.125	5.4	0.49±0.09					
125	NGC 4736	192.686	41.151	4.5	0.50±0.11	5.0		40.33	LINER	
126	NGC 4748	193.078	-13.415	5.9	0.95±0.16		0.015	42.84	NLS1	
127	**IGR J12546+1139**	193.672	11.663	4.6	0.27±0.06		0.873	46.18	Blazar	RX J1254.6+1141, QSO B1252+119
128	3C 279	194.025	-5.806	11.9	1.10±0.09		0.536	46.28	Blazar	
129	Coma Cluster	194.892	27.932	13.0	1.18±0.09		0.023	43.34	Cluster	
130	SWIFT J1300.1+1635	195.072	16.545	4.7	0.35±0.08		0.080	43.93	Sy1	2MASX J13000533+1632151
131	Mrk 783	195.741	16.396	12.7	0.97±0.08		0.067	44.21	NLS1	
132	NGC 4941	196.042	-5.569	6.9	0.70±0.10	21.2		41.73	Sy2	
133	NGC 4939	196.067	-10.347	8.3	1.15±0.14	38.8	0.010	42.62	Sy2	
134	IGR J13091+1137	197.288	11.641	27.1	1.98±0.07		0.025	43.64	XBONG	NGC 4992
135	**IGR J13100+0830**	197.507	8.508	4.1	0.29±0.07					
136	IGR J13133–1109	198.319	-11.177	4.1	0.68±0.17		0.034	43.45	Sy1	2MASX J13130580-1107424
137	NGC 5033	198.357	36.583	5.2	0.64±0.12	18.7		41.58	Sy1.9	
138	**IGR J13142–0500**	198.557	-5.014	4.1	0.47±0.12					
139	IGR J13149+4422	198.823	44.434	8.2	1.14±0.14		0.037	43.73	Sy2	Mrk 248
140	**IGR J13169+3733**	199.237	37.553	4.1	0.54±0.13		0.195	44.95	AGN	RX J1317.0+3735, 2MASS J13170290+3735329

Continued on next page

Table 4 – continued from previous page

Id	Name[1]	R.A. deg	Dec. deg	S/N	Flux mCrab	D Mpc	z	$\log L$ erg s^{-1}	Type	Notes
141	SWIFT J1321.2+0859	200.271	8.941	7.3	0.63±0.09		0.032	43.35	LINER?	NGC 5100 NED02
142	**IGR J13310−1355**	202.756	-13.931	4.0	1.18±0.29					
143	NGC 5252	204.555	4.550	43.5	4.94±0.11		0.023	43.96	Sy1.9	
144	Mrk 268	205.300	30.392	8.8	1.18±0.13		0.040	43.82	Sy2	
145	3PBC J1342.0+3539	205.546	35.699	5.9	1.01±0.17	16.0		41.64	Sy1.9	NGC 5273
146	IGR J13466+1921	206.696	19.404	4.6	0.57±0.12		0.084	44.18	Sy1.2	2MASX J13462846+1922432
147	**IGR J13486+1554**	207.168	15.901	4.8	0.57±0.12					

[1] The names of the sources previously unknown in hard X-ray band ($17-60$ keV) are highlighted in bold. The sources in spatial confusion are indicated by star. The measured flux of the sources in spatial confusion should be taken with the caution.